Research Article Vol. 34, No. 8 / 20 Apr 2026 / Optics Express 14015
Optics EXPRESS

Silicon-photonics-compatible optomechanical oscillator operating in the low-megahertz regime

WEILIN JIN, HAILONG PI, CHUANG SUN, WANCHEN BAI, AND JIZE YAN*

School of Electronics and Computer Science, University of Southampton, Southampton, SO17 1BJ, UK
**j.yan@southampton.ac.uk*

Abstract: Integrated optical sources operating at low repetition rates are a practical requirement in distributed fibre-optic sensing (DFOS) architectures, where the pulse period is set by the round-trip delay of long fibre links rather than by arbitrary design choices. Optomechanical oscillators offer a purely optical route to low-frequency signal generation, but experimental demonstrations on silicon photonic platforms have largely concentrated on higher-frequency operation or have relied on external electronic feedback to sustain oscillation. In this work, we demonstrate a silicon-photonic optomechanical oscillator operating in the low-megahertz regime as a self-sustained optical signal source without radio-frequency driving or electronic control. The device is implemented on a silicon-on-insulator platform using a racetrack resonator with a partially suspended waveguide. Stable self-oscillation is observed at a frequency of approximately 5.86 MHz. Time-domain measurements reveal a near-sinusoidal waveform, while frequency-domain spectra show a distinct mechanical resonance with a quality factor of about 1100. By adjusting the laser cavity detuning, the oscillator transitions from a single-tone oscillation state into nonlinear dynamical regimes characterized by pronounced harmonic generation. The evolution of the output spectrum follows the behavior expected from standard optomechanical models based on phase modulation of the intracavity field. Taken together, these results indicate that low-MHz optomechanical oscillators implemented within silicon photonics are experimentally accessible and can serve as compact optical signal primitives for DFOS-oriented integrated photonic systems.

1. Introduction

Distributed fibre-optic sensing (DFOS) is widely used for monitoring physical quantities along extended fibre links [1,2]. By exploiting light scattering in optical fibres, DFOS enables distributed measurements over distances ranging from several kilometres to hundreds of kilometres. Interrogation techniques such as optical time-domain reflectometry (OTDR) and optical frequency-domain reflectometry (OFDR) have been extensively developed for this purpose [3,4]. The overall performance and scalability of DFOS systems, however, are ultimately constrained by the characteristics of the optical signal source, including its repetition frequency, stability, and system complexity.

In most DFOS implementations, probe signals are generated by a continuous-wave laser combined with external modulation units, such as electro-optic or acousto-optic modulators, to produce pulsed or frequency-swept optical signals [1,5]. Although this approach offers considerable flexibility, it also increases system size, electronic complexity, and synchronization requirements. The use of multiple discrete components further introduces calibration overhead and can reduce system robustness, which is unfavourable for compact or highly integrated sensing units [1,5,6]. These factors limit system robustness and hinder integration, particularly for

#591047 https://doi.org/10.1364/OE.591047
Journal © 2026 Received 22 Jan 2026; revised 28 Mar 2026; accepted 28 Mar 2026; published 7 Apr 2026

Optics EXPRESS

compact or distributed sensing units [7]. Consequently, alternative signal generation schemes that reduce or eliminate reliance on external RF-driven modulation are of growing interest.

Cavity optomechanical systems provide an alternative physical mechanism for optical signal generation without external RF drive [8,9]. In these systems, radiation-pressure coupling between optical fields and mechanical motion can give rise to self-sustained oscillations under suitable conditions [10,11]. The resulting oscillation is maintained by intrinsic optomechanical feedback and directly maps mechanical motion onto the optical output [11–13]. Since the signal generation process is governed by the device's internal dynamics, optomechanical oscillators (OMOs) offer strong potential for on-chip integration and compact photonic signal sources.

Optomechanical self-oscillations have been experimentally demonstrated in a variety of platforms, including microring resonators, microdisks, and photonic crystal cavities [14–16]. In most reported cases, the mechanical oscillation frequencies lie in the tens of megahertz or higher [8,17–19]. This frequency range is primarily determined by device dimensions, optical mode confinement, and design strategies aimed at enhancing optomechanical coupling strength [19,20]. Such high-frequency operation is therefore well suited for applications that require fast mechanical response and high-speed signal processing.

However, the operating frequency of an OMO is not arbitrary when considered in the context of distributed fibre-optic sensing. In time- and frequency-domain DFOS schemes, the interval between successive probe signals defines the available measurement time window and thus the unambiguous sensing range [5,21]. Excessively high repetition rates shorten this time window, increasing the likelihood of temporal overlap between backscattered signals from different fibre locations and limiting the achievable sensing distance [1]. Operating in the low-megahertz regime is attractive from the perspective of DFOS, because longer intervals between successive probe signals can relax temporal overlap in long-range interrogation schemes. This frequency range therefore arises naturally from DFOS system requirements rather than from arbitrary design choices.

Despite the clear relevance of the low-megahertz band to DFOS, experimental studies of integrated optomechanical oscillators operating in this regime remain limited. Most existing OMO research focuses on higher-frequency operation, with device designs and experimental objectives not specifically targeting low repetition rates [13,22]. Related low-frequency studies are often pursued within microelectromechanical systems for inertial or mechanical sensing, or rely on platforms that do not combine silicon photonics compatibility with stable optomechanical self-oscillation [23,24]. As a result, systematic experimental investigations of on-chip OMOs operating in the low-megahertz band remain relatively scarce, leaving limited guidance for device design and system performance in this regime.

Based on these considerations, this work presents the design and experimental demonstration of an on-chip optomechanical oscillator operating in the low-megahertz band. The device is implemented on a silicon-on-insulator platform and employs a racetrack-shaped ring resonator compatible with silicon photonics circuits [25]. Locally suspended doubly clamped beams are incorporated into the optical path to serve as mechanical resonant elements. Under blue-detuned optical excitation, the device exhibits self-sustained optomechanical oscillation driven by radiation-pressure-induced dynamical backaction, without the need for external RF modulation or electronic feedback.

Experimental measurements show stable oscillation at a mechanical frequency of approximately 5.86 MHz. The oscillation threshold, steady-state behavior, and spectral characteristics are systematically characterized, confirming the feasibility of operating integrated optomechanical oscillators in a system-relevant low-megahertz regime. These results provide an on-chip experimental demonstration of low-megahertz optomechanical self-oscillation and establish its relevance as a compact low-repetition-rate optical source concept motivated by DFOS applications.

Optics EXPRESS

2. Device design and fabrication

The device was designed to realize self-sustained optomechanical oscillation in the low-megahertz regime, motivated by the operating requirements of distributed fibre-optic sensing (DFOS) systems. The design targets a low mechanical resonance frequency through the geometry of the suspended waveguide. The device concept follows the suspended racetrack resonator reported in [26], and in this work it is experimentally implemented to demonstrate MHz-regime optomechanical oscillation.

The optical cavity is a racetrack resonator formed by two straight sections connected by two circular bends. It is fabricated on a standard 220-nm-thick silicon-on-insulator (SOI) platform. The waveguide width is 450 nm, and the curved sections use circular bends with a radius of 50 μm. A locally suspended straight section is incorporated into the cavity and serves simultaneously as the mechanical resonator. This suspended beam has a length of 22 μm, a width of 450 nm, and a thickness of 220 nm, forming a high-aspect-ratio doubly clamped structure. The 22 μm dimension denotes the length of the suspended straight section.

The design parameters were selected from both optical and mechanical considerations (Fig. 1). The silicon thickness was defined by the SOI platform, and the waveguide width was chosen to support single-mode TE operation in the telecommunications band. The circular bends with a radius of 50 μm were used to maintain good optical cavity performance. The suspended beam length served as the main parameter for setting the mechanical response, and a 22 μm suspended section was used to place the fundamental mechanical resonance in the low-MHz range relevant to DFOS applications. The overall cavity size was also selected to provide a free spectral range (FSR) of approximately 0.99 nm, which supports clear identification of adjacent resonances and experimental selection of the operating point.

The suspended geometry enables coupling between the intracavity optical field and the out-of-plane motion of the beam, so that mechanical displacement modulates the effective optical path length of the resonator. Under blue-detuned excitation, radiation-pressure-induced dynamical backaction provides positive feedback and drives self-sustained oscillation, with the oscillation frequency determined primarily by the mechanical eigenmode.

The device was fabricated using CMOS-compatible processes, including electron-beam lithography, anisotropic reactive-ion etching, and selective vapor-phase hydrofluoric acid release of the buried oxide beneath designated regions. The long and narrow suspended beam used here is sensitive to fabrication nonuniformity, residual stress, and release-induced deformation. The release conditions were optimized to obtain mechanically compliant suspended beams while preserving optical integrity. The dry release process reduces the risk of stiction and structural collapse. Scanning electron microscope images of the fabricated device and a schematic of the fabrication flow are shown in Fig. 2.

3. Experimental setup and measurement methods

Experimental characterization of the optomechanical oscillator was carried out under vacuum conditions to suppress air damping and enhance the mechanical quality factor. The measurement setup is schematically illustrated in Fig. 3. A tunable continuous-wave (CW) laser was first polarization-conditioned and then amplified using an erbium-doped fiber amplifier (EDFA). The amplified optical signal was coupled into the chip through a fiber feedthrough and delivered to the on-chip resonator inside the vacuum chamber. The EDFA and high-vacuum environment used in the experiments are laboratory conditions to facilitate device characterization and stable oscillation.

Precise optical coupling was achieved using a piezo-controlled XYZ positioning stage, which enabled alignment of the input fiber to the on-chip grating couplers. The measured fiber-to-chip coupling efficiency was approximately 15%. During all measurements, the chamber pressure

Optics EXPRESS

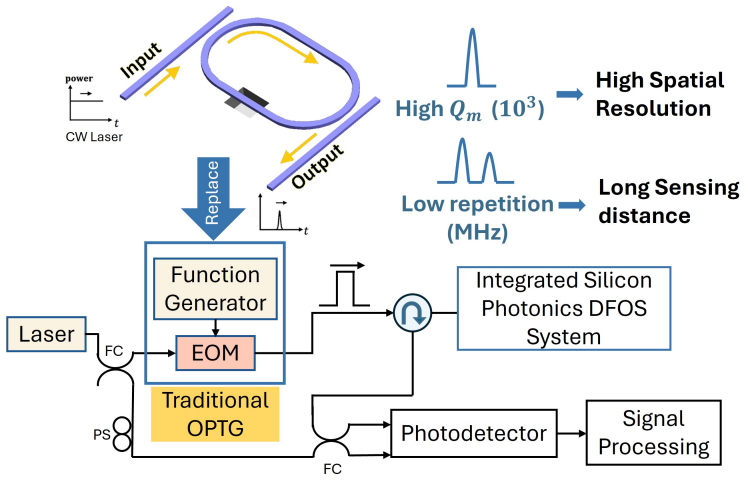

Fig. 1. Conceptual comparison between a conventional DFOS optical pulse generation scheme and the proposed optomechanical approach. In conventional systems, optical pulses are generated from a continuous-wave (CW) laser using an electro-optic modulator (EOM) driven by an external RF source such as a function generator. In the proposed chip-scale optomechanical oscillator (OMO), a CW laser is injected into the cavity and a self-sustained optical pulse train is generated through optomechanical oscillation. The OMO therefore provides an alternative on-chip pulse generation mechanism without external RF modulation units. FC: fibre coupler; PS: polarisation scrambler.

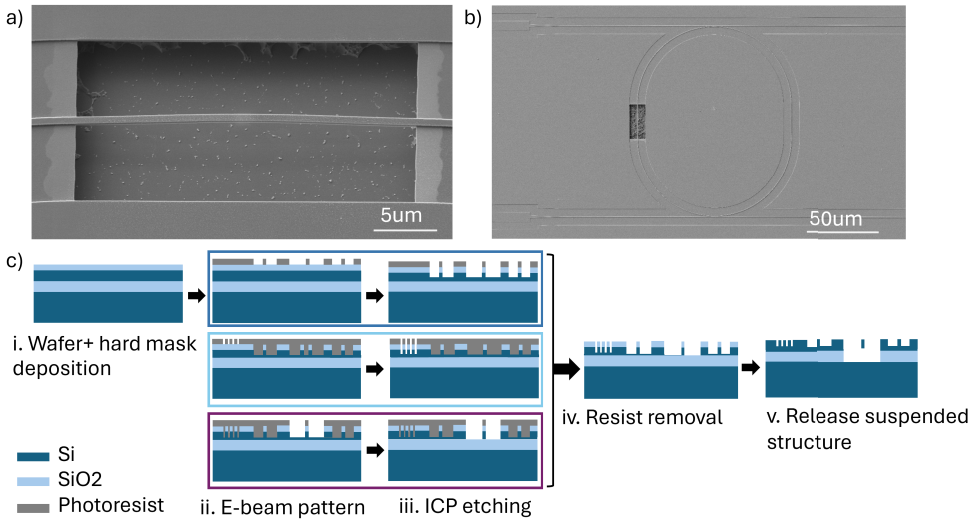

Fig. 2. **(a)** SEM image of the fabricated suspended waveguides. **(b)** Top-view SEM image of the complete resonator with bus waveguides. **(c)** schematic of the CMOS-compatible fabrication process, including lithography, ICP etching, and vapor HF release. The intermediate lithography and etching processes are performed three times each. Different colored boxes indicate different process objectives: dark blue for rib waveguide fabrication, light blue for grating coupler fabrication, and purple for strip waveguide fabrication.

Optics EXPRESS

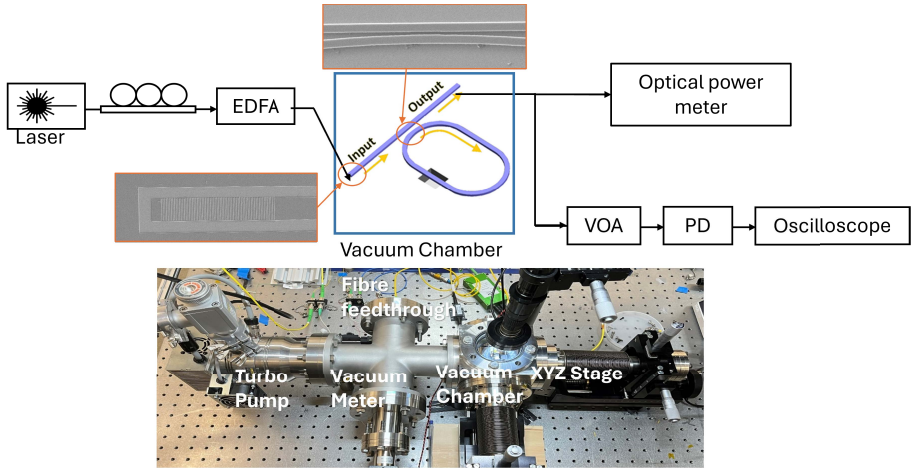

Fig. 3. Experimental setup for the optomechanical oscillator. A tunable continuous-wave (CW) laser is polarization-conditioned and amplified by an erbium-doped fiber amplifier (EDFA). The input light is coupled into the suspended resonator inside a vacuum chamber through a fiber feedthrough, with fiber alignment controlled by a piezo-driven XYZ stage. The chamber pressure is maintained at 10^{-6} mbar using a turbomolecular pump and monitored by a vacuum gauge. The optical output is directed either to an optical power meter for transmission monitoring or to a photodetector (PD) through a variable optical attenuator (VOA). The detected signal is analyzed by a high-bandwidth oscilloscope for time- and frequency-domain characterization.

was maintained at 10^{-6} mbar using a turbomolecular pump backed by an ion pump, as monitored by a vacuum gauge. The measurements were performed under such high vacuum to reduce air damping and increase the mechanical quality factor of the resonator.A microscope objective mounted above the chamber provided visual inspection and facilitated stable long-term alignment.

The optical output from the chip was routed either to an optical power meter for monitoring the average transmission or to a high-speed photodetector (PD) for dynamic signal analysis. A variable optical attenuator (VOA) was inserted before the PD to prevent detector saturation at high optical powers. The electrical signal from the PD was recorded using a high-bandwidth oscilloscope for time-domain measurements and further analyzed in the frequency domain to extract oscillation spectra and stability metrics.

In the current laboratory proof-of-concept, bulk equipment is utilized, including an external vacuum pump consuming about 110 W and an EDFA consuming about 72 W, whose power exceeds that of traditional RF modulators. However, future transitions to an integrated platform utilizing chip-scale vacuum packaging [27–29] will eliminate the need for active pumping. Furthermore, the accompanying improvements in fiber-to-chip coupling efficiency are expected to bypass the need for an EDFA, realizing low power consumption and a compact footprint. Within this context, the fully optical measurement configuration enables direct observation of self-sustained optomechanical oscillations without external RF driving or electronic feedback, while also providing access to both the temporal waveform and spectral response of the oscillator, thereby establishing the experimental basis for the results presented in the following section.

Optics EXPRESS

4. Experimental results

4.1. Self-sustained oscillation without external driving

Finite-element simulations were performed to identify the mechanical eigenmodes of the suspended beam and to support the assignment of the measured resonance peaks. The simulated displacement profiles are shown as insets in Fig. 4(a). For completeness, the measured resonance frequencies, linewidths, and quality factors of the observed modes are summarized in Table S1 in the Supplement 1. The measured optical transmission spectrum shows a resonance at 1533.06 nm with a 3-dB linewidth of 0.06 nm, corresponding to an optical quality factor of $Q \approx 25{,}000$ (Fig. 4(b)) [30]. The coupling regime of the cavity was identified by fitting the measured through-port transmission spectrum with a standard temporal coupled-mode model. From the fitting, the intrinsic quality factor Q_0 and coupling quality factor Q_c were extracted separately. Since the fitted parameters satisfy $Q_0 < Q_c$ (equivalently, $\kappa_{ex} < \kappa_0$) [31], the device is confirmed to operate in the under-coupled regime.

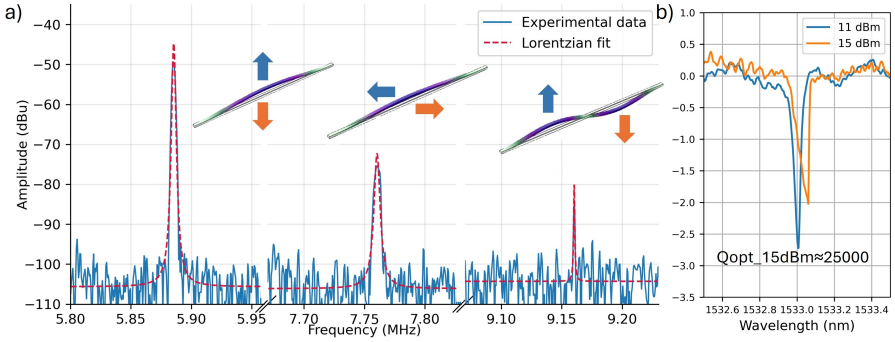

Fig. 4. Experimental characterization of the integrated optomechanical oscillator. (a) Mechanical spectra showing resonances at 5.87, 7.77, and 9.16 MHz. The dashed red curves represent Lorentzian fits. Insets illustrate the corresponding simulated flexural mode shapes. (b) Optical transmission spectra of the racetrack resonator measured at input powers of 11 and 15 dBm. The resonance exhibits a loaded optical quality factor of approximately $Q_{opt} \approx 2.5 \times 10^4$ at 15 dBm. A power-dependent resonance redshift and lineshape distortion are observed with increasing input power, consistent with thermally induced nonlinear cavity response in the silicon resonator.

As the input power increases, the resonance exhibits a progressive redshift together with an increasingly asymmetric lineshape, indicating a thermally induced nonlinear cavity response. Similar behavior has been reported in thermally nonlinear or bistable microring resonators [32]. Figure 4(b) highlights this power-dependent resonance distortion.

To investigate the dynamic behavior of the integrated OMO, the input laser power was fixed at 15 dBm and the laser wavelength was tuned to the blue-detuned side of the optical resonance. The operating point was chosen on the right-hand slope near 1533.06 nm, where optomechanical transduction is strong while thermal instability is reduced [8,33]. Under these experiment setting, the cavity linewidth remains much broader than the mechanical frequency ($\kappa \gg \Omega_m$, with $\Omega_m/2\pi \approx 5.86$ MHz), indicating operation in the unresolved-sideband regime. For the present low-MHz implementation, this regime arises from the combination of optical linewidth and mechanical frequency, and relaxes the requirement on the optical quality factor while supporting stable self-sustained oscillation.

Under these conditions, the system enters a regime of self-sustained optomechanical oscillation driven by intrinsic radiation-pressure backaction. Figure 5(a) shows the time-domain signal

Optics EXPRESS

measured with a 125 MHz photodetector, together with a sinusoidal fit illustrating the near-sinusoidal oscillation waveform. The frequency-domain response in Fig. 5(b) shows a sharp oscillation peak at 5.86 MHz, matching the fundamental mechanical mode identified in Fig. 4(a). These results demonstrate stable self-sustained optomechanical oscillation in the low-megahertz regime of interest for low-repetition-rate source concepts.

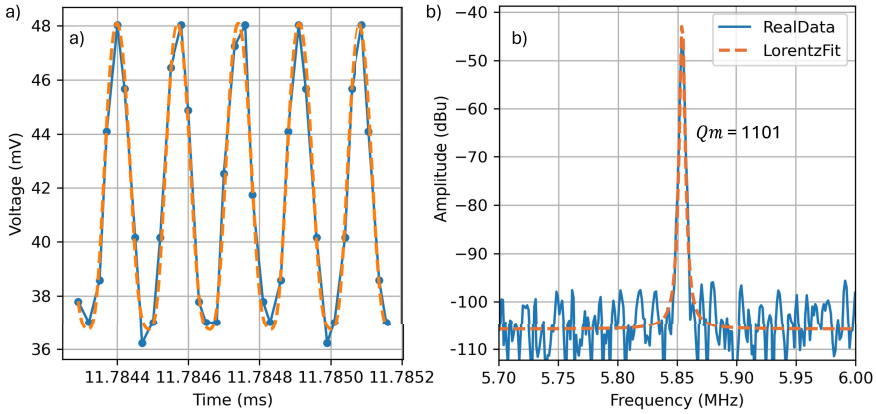

Fig. 5. Experimental characterization of the integrated optomechanical oscillator. (a) Time-domain oscillation signal (blue) measured using a 125 MHz bandwidth photodetector, together with a sinusoidal fit (orange). The time-domain trace in this figure was recorded with an oscilloscope sampling rate of 39.1 MS/s. (b)Frequency-domain response showing a sharp oscillation peak at 5.86 MHz (blue), with a Lorentzian fit (orange) yielding a mechanical quality factor of $Q_{\mathrm{m}} \approx 1100$. No significant higher-order harmonics are observed.

4.2. Harmonic generation and nonlinear waveform transitions

To study the onset of nonlinear dynamics, the pump wavelength was incrementally tuned deeper into the blue-detuned side of the resonance while maintaining 15 dBm input power. At each step ($\Delta\lambda = 0.001$ nm), both the time-domain waveform and the corresponding power spectral density (PSD) were recorded.

As detuning increased, the oscillator evolved from a near-sinusoidal state into a nonlinear regime marked by new spectral components. Figure 6 shows a representative PSD: in addition to the 5.86 MHz fundamental, strong peaks appeared at 11.7 MHz and 17.5 MHz. These components are absent near the threshold and emerge at stronger detuning, which is consistent with theoretical predictions reported in [9,34], indicating a nonlinear origin.

With further increase in detuning, the oscillator not only exhibited stronger nonlinear spectral features, but also showed a gradual reduction in overall oscillation amplitude. Beyond this point, the oscillation eventually disappeared once the effective optical gain could no longer compensate mechanical damping, consistent with the theoretical framework of radiation-pressure-induced dynamical multistability [8,9]. This behavior highlights the dual role of detuning in the present device: while it enables optomechanical gain to sustain oscillation, it also defines the stability boundary of accessible dynamical states. These nonlinear effects arise naturally once stable low-MHz oscillation is established and do not require additional actuation or system complexity.

Overall, these results show that laser detuning provides a practical means to control the spectral content and operating regime of the oscillator. These observations are consistent with the theoretical analysis presented in Section 5, which provides a physical interpretation of the observed nonlinear behavior.

Optics EXPRESS

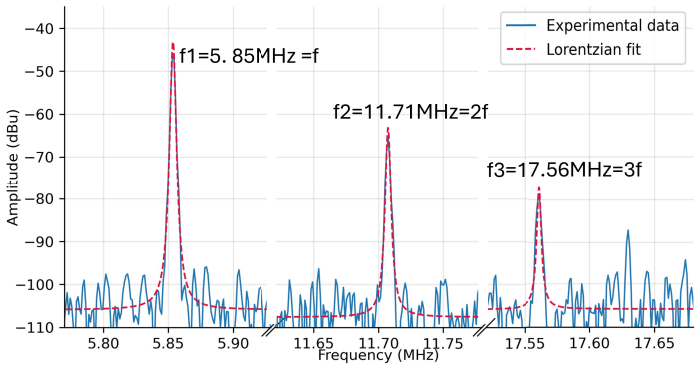

Fig. 6. Power spectral density of the oscillator output under blue-detuned pumping. The fundamental oscillation peak appears at $f_1 = 5.86$ MHz, while clear higher-order components are observed at $f_2 = 11.71$ MHz ($2f$) and $f_3 = 17.56$ MHz ($3f$). The emergence of these second- and third-order harmonics confirms the nonlinear regime of the optomechanical oscillator. A Lorentzian fit (dashed line) is included for comparison with the experimental data (solid line).

5. Theoretical modeling and analysis

5.1. Modeling and oscillation threshold

The behavior of an optomechanical oscillator can be described within the standard coupled-mode framework [8,10], which captures the interaction between the intracavity optical field and the mechanical displacement of the resonator. The intracavity field amplitude $a(t)$ evolves as

$$\dot{a}(t) = \left(i\Delta - \frac{\kappa}{2}\right) a(t) - ig_0 x(t)a(t) + \sqrt{\kappa_e} s_{in}(t), \tag{1}$$

where $\Delta = \omega_L - \omega_c$ is the laser–cavity detuning, κ is the total optical linewidth, g_0 is the vacuum optomechanical coupling rate, and $s_{in}(t)$ denotes the input field. The mechanical mode, with effective mass m, resonance frequency Ω_m, and damping rate Γ_m, follows

$$m\ddot{x}(t) + m\Gamma_m \dot{x}(t) + m\Omega_m^2 x(t) = \hbar g_0 |a(t)|^2, \tag{2}$$

where the right-hand side represents the radiation-pressure force generated by intracavity photons. Together, these equations describe the feedback mechanism responsible for optomechanical self-oscillation once the oscillation threshold is exceeded.

In the present work, this established framework is used to provide a physical interpretation of the experimentally observed oscillation behavior. Since the detailed normalization and derivation are well documented elsewhere [33], only the aspects directly relevant to the present device are discussed here.

At low input powers, the mechanical mode remains thermally driven and no coherent oscillation occurs. As the optical power increases, radiation-pressure-induced dynamical backaction modifies the effective mechanical damping [35]. In addition to altering the damping, dynamical backaction also changes the effective mechanical stiffness, leading to a detuning-dependent shift of the mechanical resonance frequency, commonly referred to as the optical spring effect [8]. Its possible contribution to the experimentally observed frequency offset is discussed later in this section.

Following the dimensionless treatment in [33], the oscillation threshold power can be estimated, up to a dimensionless factor depending on the laser–cavity detuning and coupling efficiency, as

$$P_{th} \propto \frac{\kappa^2}{g_0^2 Q_m}, \tag{3}$$

Optics EXPRESS

where $Q_m = \Omega_m/\Gamma_m$ is the mechanical quality factor [8]. This scaling highlights that a smaller optical linewidth, stronger optomechanical coupling, and higher mechanical quality factor reduce the required pump power. A more complete expression for the threshold power, including the explicit dependence on detuning and coupling efficiency, is provided in Supplement 1.

The present device operates in the unresolved-sideband regime, with $\kappa \gg \Omega_m$, owing to the combination of the measured optical linewidth and the low-megahertz mechanical frequency. In this regime, the intracavity field follows the mechanical motion quasi-instantaneously, so radiation-pressure feedback remains effective for driving self-sustained oscillation. Although unresolved-sideband operation is not optimal for applications such as sideband cooling, it is fully compatible with the present objective of demonstrating stable low-frequency optomechanical oscillation.

In the experiments, an input power of 15 dBm was selected as the operating condition. This value was chosen to remain above the threshold level estimated from the scaling in Eq. (3), based on the measured optical linewidth and mechanical quality factor. The agreement supports the interpretation that the onset of oscillation is governed by the combined effects of cavity photon lifetime, optomechanical coupling strength, and mechanical dissipation, in accordance with the coupled-mode description.

5.2. Nonlinear dynamics: harmonic generation

Once the pump power exceeds the oscillation threshold, the optomechanical oscillator exhibits nearly sinusoidal motion at the fundamental frequency Ω_m. As the laser detuning is increased further into the blue-detuned side of the cavity resonance, the oscillation amplitude grows and the system gradually enters a nonlinear regime. A characteristic signature of this transition is the appearance of higher-order harmonics in the output spectrum.

In steady state, the mechanical displacement can be approximated as

$$x(t) = A\cos(\Omega_m t), \tag{4}$$

where A denotes the oscillation amplitude. This periodic displacement modulates the cavity resonance frequency and introduces phase modulation into the intracavity optical field. The modulation can be expressed as $\exp[i\beta\cos(\Omega_m t)]$, where the modulation index β is proportional to A. Using the Fourier–Bessel expansion,

$$e^{i\beta\cos(\Omega_m t)} = \sum_{n=-\infty}^{\infty} i^n J_n(\beta) e^{in\Omega_m t}, \tag{5}$$

the optical field is seen to contain frequency components at integer multiples $n\Omega_m$ of the mechanical resonance frequency. In particular, the terms involving $J_2(\beta)$ and $J_3(\beta)$ correspond to second- and third-order harmonics at $2\Omega_m$ and $3\Omega_m$.

This description is consistent with the experimentally observed spectra. For the present device, the fundamental oscillation occurs at 5.86 MHz, while additional peaks at 11.8 MHz and 17.7 MHz appear under stronger blue detuning, corresponding to the second and third harmonics. These higher-order components are absent close to threshold and emerge only at larger oscillation amplitudes, indicating that nonlinear phase modulation of the cavity field by mechanical motion plays a dominant role.

5.3. Consistency with experimental observations and implications

The coupled-mode analysis captures the essential features observed experimentally and provides a consistent physical interpretation of the measured oscillation behavior. Using the threshold condition in Eq. (3) together with the measured cavity parameters, the theoretical oscillation threshold is estimated to be approximately 10.3 dBm. The 15 dBm input power used in our

Optics EXPRESS

measurements (Section 4.2) was selected to make sure the device operated well above this threshold, so that self-sustained oscillation could be clearly observed. Based on the same threshold condition, the vacuum optomechanical coupling rate is estimated to be on the order of $g_0/2\pi \approx 39$ kHz. The analysis is also consistent with the experimentally observed operation in the unresolved-sideband regime, where radiation-pressure feedback remains sufficient to sustain coherent oscillation at 5.86 MHz.

Under these conditions, dynamical backaction can also shift the effective mechanical resonance frequency through the optical spring effect. Based on the measured optical linewidth of $\kappa/2\pi \approx 7.66$ GHz, the estimated vacuum optomechanical coupling rate, and representative intracavity photon numbers, an order-of-magnitude estimate indicates that a frequency shift on the order of several tens of kilohertz is plausible in the self-oscillation regime. This estimated scale is consistent with the frequency offset observed between the mechanically identified resonance in Fig. 4 and the oscillation peak measured under the selected operating condition in Fig. 5. Details of the corresponding derivation are provided in the Supplement 1 S3.

The nonlinear analysis likewise aligns with the experimental observations. The Fourier–Bessel expansion predicts harmonic components at integer multiples of the mechanical frequency, which correspond directly to the peaks observed at $2\Omega_m$ and $3\Omega_m$ in the measured spectra. These results indicate that the observed nonlinear behavior arises naturally from large-amplitude mechanical motion and does not require additional system complexity.

Taken together, the agreement between experiment and theory indicates that the standard coupled-mode framework is sufficient to interpret the behavior of the present device. Importantly, the analysis supports the experimental conclusion that low-frequency optomechanical oscillators can operate stably within system-relevant conditions for sensing-oriented photonic architectures, such as distributed fibre-optic sensing systems. The results further highlight that cavity photon lifetime, optomechanical coupling strength, and mechanical quality factor jointly determine the accessible oscillation regimes, while laser detuning provides a practical control parameter for tailoring the spectral content of the oscillation.

6. Discussion and conclusion

This work demonstrates optomechanical self-oscillation on a silicon photonic platform operating in the low-megahertz regime. The operating frequency demonstrated here lies well below that of most reported optomechanical oscillators, but it matches the temporal scale imposed by distributed fibre-optic sensing (DFOS) systems. In time-domain interrogation schemes such as optical time-domain reflectometry, the repetition rate of the optical signal sets the available measurement window and therefore limits the unambiguous sensing range. In practical DFOS architectures, this range is defined by the pulse or burst repetition rate, which typically lies in the kilohertz regime for kilometer-scale links, rather than by the intra-burst modulation frequency [26]. From this viewpoint, the device presented in this work is not designed to directly determine sensing distance or to replace a complete DFOS interrogator. Instead, it provides an integrated optical signal primitive whose intrinsic dynamics are compatible with system-level timing requirements.

When viewed at the system level, the optomechanical oscillator functions as a compact source of low-frequency optical modulation that can be embedded at the chip scale [30,36]. Compared with conventional solutions based on electro-optic or acousto-optic modulation, this approach reduces reliance on externally driven modulation and associated RF synchronization, as well as the need for high-speed electronic drivers. The resulting reduction in circuit complexity is particularly relevant for compact or distributed sensing nodes, where electronic overhead and long-term robustness often become limiting factors. In this sense, the present results establish feasibility rather than completeness, and deliberately avoid prescribing a specific interrogation architecture.

Optics EXPRESS

Experimentally, stable self-sustained oscillation is observed in the low-megahertz band, with a clear periodic waveform and a narrow spectral peak corresponding to a mechanical quality factor of approximately $Q_{\mathrm{m}} \approx 1100$. This indicates that the oscillation state remains dynamically stable under steady operating conditions. The measured mechanical quality factor is sufficient to sustain stable oscillation and is not optimized in the present design. At the same time, it is well understood that the spectral purity of optomechanical oscillators is influenced by multiple noise sources, including thermomechanical fluctuations, photon shot noise, and technical noise from the optical drive [17,37,38]. These contributions depend strongly on detuning, optical power, and device geometry. For sensing-oriented applications, a detailed analysis of phase noise and long-term drift under realistic environmental conditions will therefore be necessary and has not been addressed here. In this study, the experiments were carried out in a high-vacuum environment to enable stable self-sustained oscillation of the present device. Under ambient conditions, stronger air damping is expected to significantly reduce the mechanical quality factor and increase the oscillation threshold. Based on a threshold-scaling analysis using a literature low-Q reference as an illustrative case [39], the ambient-pressure threshold is estimated to be on the order of 20.7 dBm, which is large than the maximum optical power delivered to the device in the present setup. Therefore, the self-oscillation in ambient pressure was not achieved in our current setup, which can be explored in the future. Stable cavity operation without apparent damage was maintained up to the maximum tested input power of 20 dBm. The ultimate optical damage threshold of the device was not determined in the present study and could be investigated in future work.

In conclusion, a silicon-photonics-compatible optomechanical oscillator operating as a self-sustained optical signal source in the low-megahertz regime has been demonstrated. The combination of on-chip integration and system-relevant operating frequency defines a physical platform for compact optical signal generation under timing constraints typical of distributed fibre-optic sensing. Beyond this immediate context, the observed access to nonlinear dynamical behaviour and harmonic generation through optical detuning points to a broader role for low-frequency optomechanical oscillators in integrated photonic signal processing and waveform control.

Funding. Engineering and Physical Sciences Research Council (Grant No.~EP/V000624/1).

Disclosures. The authors declare no conflicts of interest.

Data availability. Data underlying the results presented in this paper are not publicly available at this time but may be obtained from the authors upon reasonable request.

Supplemental document. See Supplement 1 for supporting content.

References

1. A. H. Hartog, *An introduction to distributed optical fibre sensors* (CRC press, 2017).
2. P. Lu, N. Lalam, M. Badar, *et al.*, "Distributed optical fiber sensing: Review and perspective," Appl. Phys. Rev. **6**(4), 041302 (2019).
3. Y. Lu, T. Zhu, L. Chen, *et al.*, "Distributed vibration sensor based on coherent detection of phase-otdr," J. Lightwave Technol. **28**(22), 3243–3249 (2010).
4. M. Wegmuller, J. Von Der Weid, P. Oberson, *et al.*, "High resolution fiber distributed measurements with coherent ofdr," in *Proc. ECOC'00*, vol. 11 (Munich, Germany, 2000), p. 109.
5. A. Gowshikan, K. Kariyawasam, X. Xu, *et al.*, "A review on the advances in distributed fibre optic sensing technology for structural health monitoring," in *12th International Conference on Structural Engineering and Construction Management: Proceedings of the ICSECM 2021*, (Springer, 2022), pp. 145–159.
6. S. Liu, F. Yu, R. Hong, *et al.*, "Advances in phase-sensitive optical time-domain reflectometry," Opto-Electron. Adv. **5**(3), 200078 (2022).
7. L. Thévenaz, "Distributed optical fiber sensors: what is known and what is to come," Front. Sens. **6**, 1546392 (2025).
8. M. Aspelmeyer, T. J. Kippenberg, and F. Marquardt, "Cavity optomechanics," Rev. Mod. Phys. **86**(4), 1391–1452 (2014).
9. F. Marquardt, J. Harris, and S. M. Girvin, "Dynamical multistability induced by radiation pressure in high-finesse micromechanical optical cavities," Phys. Rev. Lett. **96**(10), 103901 (2006).
10. T. J. Kippenberg and K. J. Vahala, "Cavity opto-mechanics," Opt. Express **15**(25), 17172–17205 (2007).

Optics EXPRESS

11. M. Hossein-Zadeh and K. J. Vahala, "An optomechanical oscillator on a silicon chip," IEEE J. Sel. Top. Quantum Electron. **16**(1), 276–287 (2010).
12. M. Grimm, C. Bruder, and N. Lörch, "Optomechanical self-oscillations in an anharmonic potential: engineering a nonclassical steady state," J. Opt. **18**(9), 094004 (2016).
13. E. Gil-Santos, M. Labousse, C. Baker, *et al.*, "Light-mediated cascaded locking of multiple nano-optomechanical oscillators," Phys. Rev. Lett. **118**(6), 063605 (2017).
14. D. Van Thourhout and J. Roels, "Optomechanical device actuation through the optical gradient force," Nat. Photonics **4**(4), 211–217 (2010).
15. J. Khurgin, M. Pruessner, T. Stievater, *et al.*, "Laser-rate-equation description of optomechanical oscillators," Phys. Rev. Lett. **108**(22), 223904 (2012).
16. X. Liu, W. Liu, Z. Ren, *et al.*, "Progress of optomechanical micro/nano sensors: a review," Int. J. Optomechatronics **15**(1), 120–159 (2021).
17. X. Luan, Y. Huang, Y. Li, *et al.*, "An integrated low phase noise radiation-pressure-driven optomechanical oscillator chipset," Sci. Rep. **4**(1), 6842 (2014).
18. W. C. Jiang, X. Lu, J. Zhang, *et al.*, "High-frequency silicon optomechanical oscillator with an ultralow threshold," Opt. Express **20**(14), 15991–15996 (2012).
19. Y. Hu, S. Ding, Y. Qin, *et al.*, "Generation of optical frequency comb via giant optomechanical oscillation," Phys. Rev. Lett. **127**(13), 134301 (2021).
20. M.-A. Miri, G. D'Aguanno, and A. Alù, "Optomechanical frequency combs," New J. Phys. **20**(4), 043013 (2018).
21. M. Soriano-Amat, H. F. Martins, V. Durán, *et al.*, "Time-expanded phase-sensitive optical time-domain reflectometry," Light: Sci. Appl. **10**(1), 51 (2021).
22. F. Liu and M. Hossein-Zadeh, "Mass sensing with optomechanical oscillation," IEEE Sens. J. **13**(1), 146–147 (2013).
23. B. Guha, P. E. Allain, A. Lemaitre, *et al.*, "Force sensing with an optomechanical self-oscillator," Phys. Rev. Appl. **14**(2), 024079 (2020).
24. K. Han, J. H. Kim, and G. Bahl, "Aerostatically tunable optomechanical oscillators," Opt. Express **22**(2), 1267–1276 (2014).
25. G. T. Reed and A. P. Knights, *Silicon photonics: an introduction* (Wiley Online Library, 2004).
26. X. Xu, "Integrated silicon optomechanical system and its applications," Ph.D. thesis, University of Southampton (2021).
27. "High-resolution strain sensing on steel by silicon-on-insulator flexural resonators fabricated with chip-level vacuum packaging," in *2013 Transducers & Eurosensors XXVII: The 17th International Conference on Solid-State Sensors, Actuators and Microsystems (TRANSDUCERS & EUROSENSORS XXVII)*, (IEEE, 2013), pp. 992–995.
28. L. Belsito, M. Ferri, F. Mancarella, *et al.*, "Fabrication of high-resolution strain sensors based on wafer-level vacuum packaged mems resonators," Sensors Actuators A: Phys. **239**, 90–101 (2016).
29. M. Ferri, F. Mancarell, L. Belsito, *et al.*, "Strain sensing on steel surfaces using vacuum packaged mems resonators," Procedia Eng. **5**, 1426–1429 (2010). Eurosensor XXIV Conference
30. M. Bagheri, M. Poot, M. Li, *et al.*, "Dynamic manipulation of nanomechanical resonators in the high-amplitude regime and non-volatile mechanical memory operation," Nat. Nanotechnol. **6**(11), 726–732 (2011).
31. M. Soltani, "Novel integrated silicon nanophotonic structures using ultra-high q resonators," (2009).
32. K. Powell, J. Wang, A. Shams-Ansari, *et al.*, "Optical bi-stability in cubic silicon carbide microring resonators," Opt. Express **30**(19), 34149–34158 (2022).
33. X. Xu, H. Pi, W. Yu, *et al.*, "On-chip optical pulse train generation through the optomechanical oscillation," Opt. Express **29**(23), 38781–38795 (2021).
34. W. Xiong, Z. Li, G.-Q. Zhang, *et al.*, "Higher-order exceptional point in a blue-detuned non-hermitian cavity optomechanical system," Phys. Rev. A **106**(3), 033518 (2022).
35. A. Schliesser, P. Del'Haye, N. Nooshi, *et al.*, "Radiation pressure cooling of a micromechanical oscillator using dynamical backaction," Phys. Rev. Lett. **97**(24), 243905 (2006).
36. B.-B. Li, L. Ou, Y. Lei, *et al.*, "Cavity optomechanical sensing," Nanophotonics **10**(11), 2799–2832 (2021).
37. K. Y. Fong, M. Poot, X. Han, *et al.*, "Phase noise of self-sustained optomechanical oscillators," arXiv (2014).
38. A. A. Clerk, M. H. Devoret, S. M. Girvin, *et al.*, "Introduction to quantum noise, measurement, and amplification," Rev. Mod. Phys. **82**(2), 1155–1208 (2010).
39. J. Roels, B. Maes, R. Baets, *et al.*, "Integrated optomechanical circuits," in *Integrated Photonics Research, Silicon and Nanophotonics and Photonics in Switching*, (Optica Publishing Group, 2010), p. IMF4.